

A quasi-continuum hydrodynamic model for slit shaped nanochannel flow

Ravi Bhaduria and N. R. Aluru^{a)}

Department of Mechanical Science and Engineering, Beckman Institute for Advanced Science and Technology, University of Illinois at Urbana-Champaign, Urbana, Illinois 61801, USA

(Received 7 June 2013; accepted 29 July 2013; published online 19 August 2013)

We propose a quasi-continuum hydrodynamic model for isothermal transport of Lennard-Jones fluid confined in slit shaped nanochannels. In this work, we compute slip and viscous contributions independently and superimpose them to obtain the total velocity profile. Layering of fluid near the interface plays an important role in viscous contribution to the flow, by apparent viscosity change along the confining dimension. This relationship necessitates computing density profiles, which is done using the recently proposed empirical-potential based quasi-continuum theory [A. V. Raghunathan, J. H. Park, and N. R. Aluru, *J. Chem. Phys.* **127**, 174701 (2007)]. Existing correlations for density dependent viscosity provided by Woodcock [*AIChE J.* **52**, 438 (2006)] are used to compute viscosity profile in the nanopores. A Dirichlet type slip boundary condition based on a static Langevin friction model describing center-of-mass motion of fluid particles is used, the parameters of which are dependent on the fluctuations of total wall-fluid force from an equilibrium molecular dynamics simulation. Different types of corrugated surfaces are considered to study wall-fluid friction effects on boundary conditions. Proposed hydrodynamic model yields good agreement of velocity profiles obtained from non-equilibrium molecular dynamics simulations for gravity driven flow. © 2013 AIP Publishing LLC. [<http://dx.doi.org/10.1063/1.4818165>]

I. INTRODUCTION

Recent years have seen a great surge in study of fluid transport process and its mechanism at nanometer scales. It is a subject of long-standing importance pursued by many researchers due to its implications in a variety of processes such as gas separation,¹ heterogeneous catalysis,² carbon sequestration in Metal Organic Frameworks (MOF),³ water purification,⁴⁻⁷ and understanding biological flows in membranes.⁸ The early attempts to understand transport is attributed to Knudsen⁹ and Smoluchowski¹⁰ who studied molecular transport for hard sphere fluids at low densities, neglecting wall-fluid, and fluid-fluid interactions. However, these interactions play an important role in transport problem in nanopores and therefore an accurate modeling of these interactions becomes critical.¹¹

With the inclusion of fluid-surface interactions that also take into account the wall topology in the longitudinal direction, surface effects influence hydrodynamics on two different aspects. First, they result in density inhomogeneity in the direction of confinement, which leads to spatially varying, density dependent transport coefficients.^{12,13} Second, these fluid-surface interactions result in the surface friction experienced by the fluid, that affects the collective motion of the fluid particles relative to the wall, a phenomenon known as slip, which is studied both theoretically and experimentally.^{14,15} Several models for slip exist today which describe the phenomenon from different perspectives, including the surface effects and shear rate dependent models.¹⁶⁻²³ There have been instances of enhanced transport flux attributed to decrease in surface friction due to increasing shear rate.^{14,21}

Bhatia *et al.* have performed an array of studies targeting slip in meso and nano scale pores.²⁴⁻²⁷ They have developed an oscillator model for computing transport diffusion under special case of Maxwell's boundary condition, which is exact for low density fluids.²⁴ Viscous and diffusive components of flow are superimposed over each other to obtain the effective transport flux. This approach, however promising, relies on an approximation of diffuse wall boundary condition with the pore which is not always the correct representation of the wall. Furthermore, it is reported in Ref. 28 that diffusion in graphite slits can be best computed using rigid wall models. To apply their work to a defect free, rigid surfaces, Smoluchowski correction factor is introduced,²⁹ which is a complicated function of the thermodynamic state of the fluid and wall structure, and till date only limited studies exist for its calculation.^{30,31}

Recently, a statistical mechanical based model using Green-Kubo relations for calculating slip length has been presented.^{32,33} This model computes the slip length as a ratio of a phenomenological parameter, friction factor to the shear viscosity. This model can then be used in conjunction with Navier slip boundary condition²⁰ to obtain the velocity profile. Friction factor is inherently related to the fluctuations of wall fluid interaction force, which can be computed from equilibrium molecular dynamics (EMD) simulations. Hydrodynamic location of the wall is also computed using EMD correlations, where the Navier slip condition has been applied. There has been a suggestion about the limitation of this model for small pores³⁴ ($\sim 5\sigma_{ff}$, σ_{ff} being the fluid particle diameter), in which wall-fluid potential due to confining surfaces overlap.

In this work, we present a hydrodynamic model which includes both the lateral and longitudinal surface effects.

^{a)}Electronic mail: aluru@illinois.edu

Spatially varying shear viscosity in the confining direction is determined using the existing correlations for viscosity. Slip effects are modeled using a static Langevin equation describing the center-of-mass (COM) motion of fluid particles,^{35,36} with its stochastic force being the total wall-fluid interaction force in the streamwise direction computed from an EMD simulation. We observe that, under the same thermodynamic state, only one EMD simulation is required to obtain parameters of Langevin model for different channel widths. The model is used to study hydrodynamics for three systems, with differing surface-fluid friction due to relative motion between surface and fluid for slit shaped nanochannels.

The rest of the paper is organized as follows: in Sec. II we present the hydrodynamic transport model. We briefly discuss the EQT method used to calculate density profiles of fluid under confinement in slit channels. Local average density method (LADM) proposed by Bitsanis *et al.*^{12,13} is used with viscosity correlations presented by Woodcock³⁷ to obtain spatial variations of fluid viscosity as a functional of density. We also present the development of a generic boundary condition using Langevin type model. In Sec. III, necessary details of MD simulations are provided. In Sec. IV results obtained from the hydrodynamic model are discussed and compared with non-equilibrium molecular dynamics (NEMD) simulations. Finally, conclusions are drawn in Sec. V.

II. TRANSPORT MODEL

The starting point of the transport model is the Cauchy momentum equation, which relates inertial flux to the diffusive flux and is given by

$$\frac{D\rho\mathbf{u}}{Dt} = -\nabla P + \nabla \cdot \boldsymbol{\tau} + \mathbf{f}, \quad (1)$$

where $D/Dt = \partial/\partial t + \mathbf{u} \cdot \nabla$ is the material derivative, \mathbf{u} is the velocity field, ρ is the mass density of the fluid, P is the hydrostatic pressure, \mathbf{f} is the body force per unit volume. $\boldsymbol{\tau}$ is the deviatoric stress tensor, which relates to strain rate constitutive relation to obtain the Navier–Stokes equation for incompressible fluids

$$\frac{D\rho\mathbf{u}}{Dt} = -\nabla P + \nabla \cdot (\mu\nabla\mathbf{u}) + \mathbf{f}, \quad (2)$$

where μ is the dynamic viscosity. This can be further approximated for one-dimensional gravity driven low Reynolds number flow (see Fig. 1) as

$$\frac{d}{dz} \left[\mu(z) \frac{du_x(z)}{dz} \right] + mc(z)g_x = 0 \quad (3)$$

with boundary conditions

$$u_x \left(-\frac{L}{2} + \delta \right) = \left(+\frac{L}{2} - \delta \right) = u_s, \quad (4)$$

where $u_x(z)$ is the unknown streaming direction velocity, z is the direction of confinement, x is the streaming direction, m is the molecular mass of the fluid, $c(z)$ is the number density (which relates to mass density $\rho(z) = mc(z)$, and is referred as density from now on), L is the channel width, and g_x is

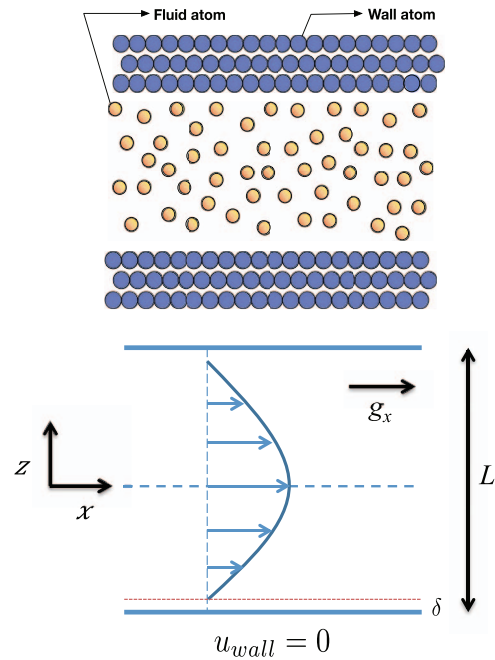


FIG. 1. Schematic plot of the gravity driven flow considered in present work.

the gravity field applied in the streaming direction. Continuity equation is already satisfied under the assumption that u_z is identically zero. Closure to the governing equations is provided by Dirichlet boundary condition at a fixed distance δ from the surface. Inputs required for this framework are density, viscosity, magnitude of slip velocity u_s , and the distance δ from the actual position of the wall, where slip condition is applied. The methods to obtain these inputs are discussed below.

A. Density profiles

We first calculate density variations along the confinement to facilitate computation of viscosity profile in the slit. Here, we use empirical-potential based quasicontinuum theory^{38–42} (EQT) to compute the density profiles. EQT is a multiscale framework for fast and accurate prediction of density profile of confined fluid. It uses a continuum formulation to model the wall-fluid and fluid-fluid interaction between the atoms, and solves for the density and total potential of mean force (PMF) inside a channel in a self-consistent manner. The inputs to the EQT framework are wall-fluid, and fluid-fluid interaction parameters, average density of fluid in the slit, and channel wall density. In EQT, for a slit like channel, as shown in Fig. 1, density variation in the channel is modeled as a one-dimensional continuum variable expressed by 1D steady-state Nernst–Planck equation,

$$\frac{d}{dz} \left(\frac{dc(z)}{dz} + \frac{c(z)}{RT} \frac{dU(z)}{dz} \right) = 0 \quad (5)$$

with boundary conditions and integral constraint on average channel density as

$$c \left(-\frac{L}{2} \right) = c \left(+\frac{L}{2} \right) = 0, \quad (6a)$$

$$\frac{1}{L} \int_{-L/2}^{+L/2} c(z) dz = c_{\text{avg}}, \quad (6b)$$

where $U(z)$ is the total PMF, T is the fluid temperature, R is the ideal gas constant, and c_{avg} is the average number density of the fluid in the slit, which depends upon the thermodynamic state of the fluid, i.e., operating temperature and pressure.

The total PMF has two components, namely, wall-fluid (U^{wf}) and fluid-fluid (U^{ff}) PMF, resulting from interactions of wall-fluid and fluid-fluid particles, respectively, and is given by $U = U^{\text{wf}} + U^{\text{ff}}$. Wall-fluid PMF is computed from the continuum approximation of the wall, obtained by suitable integration taking into account the wall structure and density (c_{wall}), and wall-fluid interaction parameters,⁴³ as shown in Eq. (7a). Similarly, fluid-fluid PMF in EQT can be computed by integrating the potential between the fluid particles, weighted by the fluid density, as in Eq. (7b),

$$U^{\text{wf}}(z) = \int_V u^{\text{wf}}(|z - r|) c_{\text{wall}}(r) dV, \quad (7a)$$

$$U^{\text{ff}}(z) = \int_V u^{\text{ff}}(|z - r|) c(r) dV, \quad (7b)$$

where u^{wf} and u^{ff} are wall-fluid and fluid-fluid pair potentials, dV is the infinitesimal volume element centered at r , and $c(r)$ is the fluid number density in the volume V , outside of which, interactions between particles is neglected. A Lennard–Jones (LJ) pair potential that describes interaction between two particles, i and j of same or different species (wall and fluid), separated at distance r is written as

$$u_{\text{LJ}}^{ij}(r) = \frac{C_{12}^{ij}}{r^{12}} - \frac{C_6^{ij}}{r^6}, \quad (8)$$

where $C_{12} = 4\epsilon_{ij}\sigma_{ij}^{12}$ and $C_6 = 4\epsilon_{ij}\sigma_{ij}^6$ are LJ potential parameters. Since LJ potential is highly repulsive at small distances, computation of fluid–fluid potential may suffer from numerical singularities, leading to spurious results, or may be rendering a very stiff, and in many cases unsolvable system of equations. To avoid this, the repulsive core is “softened” by the introduction of structurally consistent smooth potential functions and bridging them with the usual 12–6 form of the LJ potential. The fluid–fluid interactions used in this work can be summarized as³⁹

$$u^{\text{ff}}(r) = \begin{cases} 0 & r < R_{\text{crit}} \\ \sum_{n=0}^2 a_n r^n & R_{\text{crit}} \leq r < R_{\text{min}} \\ u_{\text{LJ}}^{\text{ff}}(r) & R_{\text{min}} \leq r < R_{\text{cut}} \\ 0 & r \geq R_{\text{cut}} \end{cases}. \quad (9)$$

Here R_{crit} and R_{min} are parameters that define the softer repulsion and truncated core and can be obtained using an optimization algorithm. C^2 type continuity, which implies the two bridge potentials, and their first and second derivatives have the same value at R_{min} is ensured to uniquely identify the parameters a_n , as discussed in Ref. 39. Further discussion on these parameters and their values are provided in Sec. IV.

B. Viscosity profiles

In this section, we discuss the incorporation of viscosity variation into the hydrodynamic model. Since density in the slit channel varies with position, we capture the viscosity as a density dependent property. Density variations are used to estimate the local thermodynamic state of the fluid in confinement, and correlations for shear viscosity for bulk fluid are mapped to obtain the local viscosity. Bitsanis *et al.* were among the first to investigate from MD simulations the effect of density variation in velocity profiles obtained from Couette flow.¹² Few salient features of their work are

1. Viscosity must be a local function of position in the confining direction to account for the observed nonlinearity in velocity profiles.
2. Density variation along the confining direction is correlated to the observed velocity profile.
3. Density profiles do not change significantly for a transport (NEMD) simulation as compared to an equilibrium (EMD) simulation for the amount of shear rates of practical interest.

Based on the above observations, the authors proposed LADM which states that the local shear viscosity, instead of being a direct function of density $c(z)$, is a function of the local average number density $\bar{c}(z)$, which is defined as

$$\bar{c}(\mathbf{r}) = \frac{6}{\pi\sigma_{\text{ff}}^3} \int_{|\mathbf{r}-\mathbf{r}'| < \sigma_{\text{ff}}/2} c(\mathbf{r}') d^3\mathbf{r}'. \quad (10)$$

This “coarse-grained” local average density identifies a unique homogeneous (bulk) state of confined inhomogeneous fluid at a particular location in the confinement. Further accurate modeling for local average density involves averaging density profile at each point with appropriate weight functions,⁴⁴ where the definition of local average density becomes

$$\bar{c}(\mathbf{r}) = \int_{|\mathbf{r}-\mathbf{r}'| < \sigma_{\text{ff}}/2} \omega(|\mathbf{r}-\mathbf{r}'|) c(\mathbf{r}') d^3\mathbf{r}', \quad (11)$$

where the weight function ω can take various forms to deal with different thermodynamic properties of interest,^{45,46} and satisfies the normalization condition

$$\int_{|\mathbf{r}-\mathbf{r}'| < \sigma_{\text{ff}}/2} \omega(|\mathbf{r}-\mathbf{r}'|) d^3\mathbf{r}' = 1. \quad (12)$$

In this work, we choose hard-rod model⁴⁷ using which the local average density equation is written in one-dimensional form as

$$\bar{c}(z) = \frac{6}{\sigma_{\text{ff}}^3} \int_{|z-z'| < \sigma_{\text{ff}}/2} \left[\left(\frac{\sigma_{\text{ff}}}{2} \right)^2 - (z-z')^2 \right] c(z') dz', \quad (13)$$

which can then be used to obtain viscosity using suitable models for equation of state of shear viscosity. Enskog has provided a closed form expression for viscosity of fluids interacting with a hard sphere potential.⁴⁸ Similarly for LJ fluids, once an effective hard sphere diameter is calculated,⁴⁹ Enskog theory can be used to predict shear viscosity. While suitable correlations such as those given in Ref. 50 exist, there are

limitations on their applicability to different thermodynamic states. Corrections based on an accurate equation of state for LJ fluid have been proposed in Ref. 51, but they require empirical constants, which are different for different fluids.⁵²

In this work, we adopt the method proposed by Woodcock to calculate viscosity from local average density.³⁷ A one parameter model which is valid for nearly all equilibrium states of liquid and gaseous phase for LJ fluid is used. The correlation calculates viscosity as

$$\mu(\bar{c}^*, T^*) = \mu_0(T) \left[1 + B_{\mu}^* \bar{c}^* + C_{AH}(1/T^*)^{1/3} (\bar{c}^*)^4 \right], \quad (14)$$

where $\bar{c}^* = \bar{c} \sigma_{ff}^3$ and $T^* = k_B T / \epsilon_{ff}$ are reduced local average density and temperature respectively, and k_B is the Boltzmann constant. μ_0 is the zero density limit viscosity and is computed as

$$\mu_0 = \frac{5}{16\sigma_{ff}^2} \sqrt{\frac{mk_B T}{\pi}} \frac{f_{\mu}}{\Omega^{*(2,2)}}, \quad (15)$$

where $\Omega^{*(2,2)}$ is collision integral, and f_{μ} is dependent upon collision integrals, which follow recursion relation as discussed in Ref. 53. For finite densities, additional corrections for first order dependence of viscosity on density over μ_0 is done through the addition of Rainwater-Friend coefficient⁵⁴ (B_{μ}^*) as

$$B_{\mu}^* = \sqrt{2}(1 - (T^*)^{-4} - T^*/8) \quad (16)$$

C_{AH} is the Ashurst-Hoover coefficient⁵⁵ and its value is taken as 3.025. For further details on the correlation, readers are referred to the original text given in Refs. 37 and 53.

C. Boundary condition: Langevin model

To close the model, boundary conditions are needed. In macroscale hydrodynamics, the use of “no-slip” condition is widely accepted, in which the relative motion between the surface and the fluid is not assumed. But at smaller scales, this phenomenological relation fails to hold. Fluid flow past a surface can exhibit relative motion between the surface and the fluid, a phenomenon known as slip.^{14,15} The degree of slippage depends on the nature of physical interaction between the surface and the fluid molecules. When fluid particles try to move past a surface, a friction force tries to retard their relative motion due to the trapping and hopping mechanism in surface-fluid potential energy map,^{16–18} such that the shear stress in the fluid is balanced at the interface. Topology of the surface and strength of the surface-fluid interaction relative to the applied shear gradient (Couette flow) or driving force (Poiseuille flow) dictates the slip velocity.^{19–23} We propose a model for computation of slip velocity for isothermal gravity driven flow using Langevin dynamics,^{35,36,56} which incorporates these effects into a time autocorrelation function of surface-fluid force in the streaming direction. We assume that the fluid slip is a collective motion of particles, modeled as a lumped Brownian particle in the dissipative force field of the surface. This can be written in the form of Langevin

equation^{35,36} as

$$M \frac{du}{dt} = -\eta u + F(t), \quad (17)$$

where $M = Nm$ is the mass of the lumped Brownian particle, N is the number of particles in the simulation box, u is the collective velocity, and $F(t)$ is the random force acting on the particle due to the surface in the absence of any non-equilibrium force and relates to the dissipative coefficient η from the fluctuation-dissipation theorem as

$$\eta = \frac{1}{k_B T} \int_0^{\infty} \langle F(0)F(t) \rangle dt. \quad (18)$$

Using Einstein relation,⁵⁷ collective diffusion coefficient D_c of the Brownian particle can be written as

$$D_c = \frac{k_B T}{\eta}, \quad (19)$$

which can be related to slip velocity, u_s , in NEMD via mobility, μ_{mob} , and diffusion relationship

$$\mu_{\text{mob}} = \frac{u_s}{M g_x} = \frac{D_c}{k_B T}, \quad (20)$$

where g_x is the applied gravity. The final expression for slip velocity can be written as

$$u_s = \frac{D_c M g_x}{k_B T} = \frac{(k_B T) M g_x}{\int_0^{\infty} \langle F(0)F(t) \rangle dt}. \quad (21)$$

Time autocorrelation of the total surface-fluid interaction force in the streaming direction can be computed using an equilibrium MD simulation, which is computationally less expensive to perform as compared to non-equilibrium MD simulation.^{32,33} Computation of force autocorrelation is independent of width of the nanochannel, provided they are at the same thermodynamic state. This model serves as a fast and accurate tool for calculation of the slip velocity. Slip boundary condition is applied at the location of first density peak, which is the location of PMF minimum.²⁶

III. MD SIMULATION

We consider three types of systems to represent differing levels of friction between the surface and the fluid. The working fluid in all cases is single site methane, represented as a LJ particle. For the first (low friction) system, methane confined between rigid graphene sheets is considered. For the second system, we consider rigid graphene-like structure, with the wall interaction parameter changed to that of methane ($\epsilon_{\text{ww}}/k_B = 148.1$ K). This case is similar to the one presented by Sokhan *et al.*,³¹ and results in a moderate friction type of a flow situation. For the third system, four layers of a rigid silicon wall oriented in [111] direction as presented in Refs. 58 and 59 is considered with $\epsilon_{\text{ww}}/k_B = 294.93$ K, and is representative of high friction (no-slip) type boundary. All MD simulations considered here are performed at constant temperature of 300 K with a timestep of 1 fs. Lorentz-Berthelot combination rule is used to calculate the interaction parameters of surface and fluid. The number of particles in a channel is estimated using the linear superposition

approximation,^{60,61} which provides a simpler way of computing the average density in a nanochannel. Center to center distance between the first layer of wall atoms, closest to the fluid atoms from top and bottom walls, is defined as the channel width, and this definition is used for computing the average density in the nanochannel. Simulations are performed for channel widths ranging from $20\sigma_{\text{ff}}$ to $3\sigma_{\text{ff}}$, for all the systems studied here.

MD simulations are performed with LAMMPS,⁶² with working fluid as single site methane molecule. Both wall–fluid and fluid–fluid interactions are modeled with 12–6 LJ potential (see Eq. (8)), with parameters reported in Table I. For EMD simulations, systems are equilibrated for 5 ns by simulating an NVT ensemble with Nosé–Hoover thermostat⁶³ with time constant of 0.4 ps. After that, production run for 10 ns is performed, with data collected every 0.02 ps for calculating force autocorrelation. These data are divided into 1000 similar samples of 10 ps each, and the resultant force autocorrelation is averaged by the number of samples.

TABLE I. LJ interaction parameters for surface and fluid atoms. C is carbon atom, C* is carbon atom with methane LJ energy parameter, and Si is silicon atom. Fluid is LJ methane denoted by CH₄.

Atoms	σ (nm)	ϵ (kJ/mol)
CH ₄ –CH ₄	0.3810	1.2314
C–C	0.3400	0.2328
C*–C*	0.3400	1.2314
Si–Si	0.3385	2.4522
CH ₄ –C	0.3605	0.5354
CH ₄ –C*	0.3605	1.2314
CH ₄ –Si	0.3597	1.7377

NEMD simulations are performed with the same force field parameters as for EMD simulations. In addition, a uniform gravity field is applied in the x -direction, with their magnitude 4×10^{-4} nm/ps² (for graphene wall), 2×10^{-3} nm/ps² (for modified graphene wall), and 2×10^{-3} nm/ps² (for silicon wall, except for $3\sigma_{\text{ff}}$ channel in this case, where

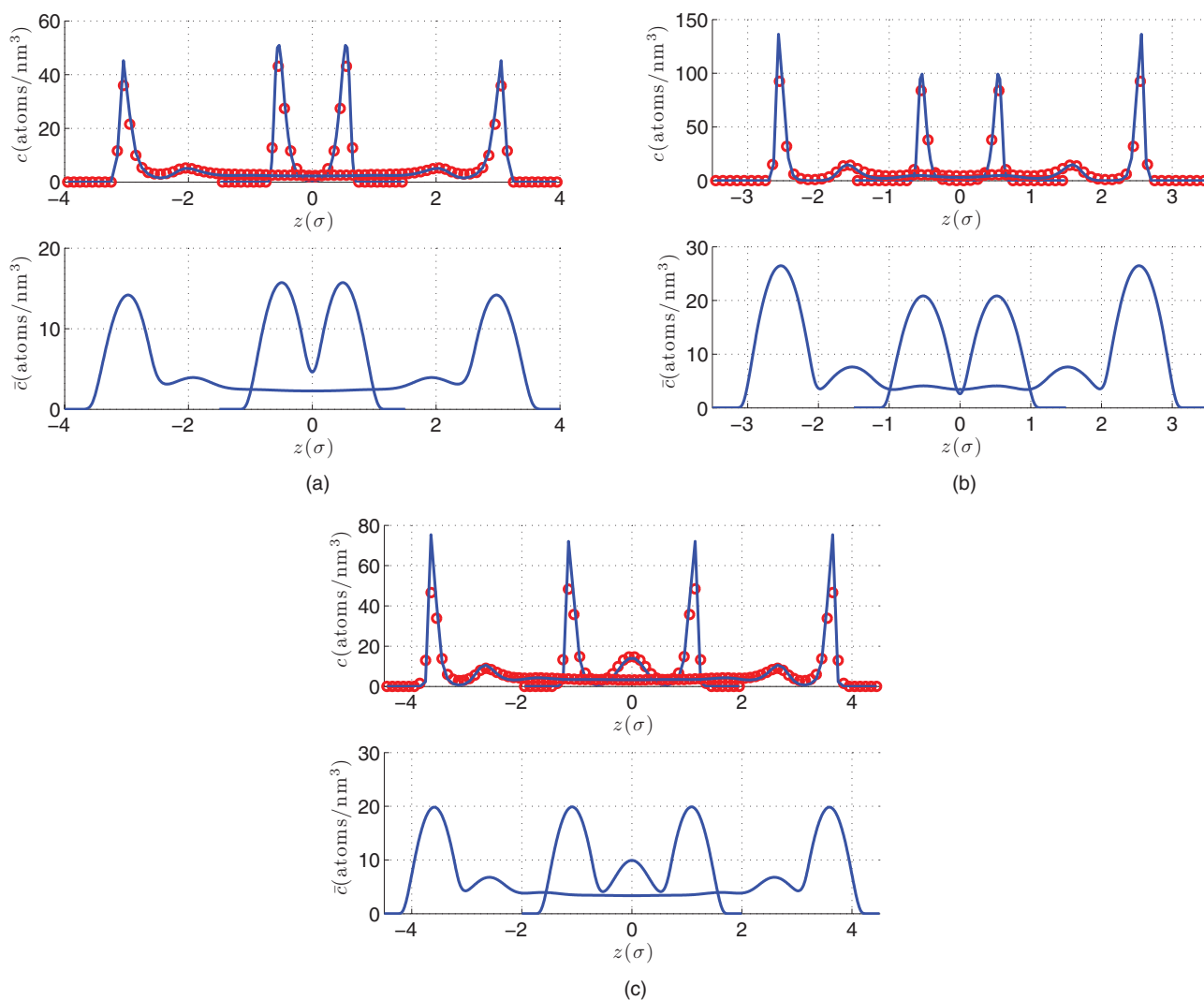


FIG. 2. Density ($c(z)$, top plot) and average density profiles ($\bar{c}(z)$, bottom plot) computed using LADM for select cases of (a) C–CH₄ ($8\sigma_{\text{ff}}$ and $3\sigma_{\text{ff}}$), (b) C*–CH₄ ($7\sigma_{\text{ff}}$ and $3\sigma_{\text{ff}}$), and (c) Si–CH₄ ($9\sigma_{\text{ff}}$ and $4\sigma_{\text{ff}}$) type systems. For density subplot, line (blue) represents EQT results, while circles (red) represent profiles from MD simulation.

5×10^{-3} nm/ps² is used for better signal-to-noise ratio). To control the temperature, we again make use of the NVT ensemble with Nosé–Hoover thermostat, only this time the thermostat is coupled to y and z directions, so that it does not interfere with the flow dynamics. We also checked that the thermostat follows the equipartition theorem, by comparing the thermal kinetic energy (computed using peculiar velocity) per particle in each direction to be equal to $k_B T/2$. This ensures that the thermostat effect is observed in each direction due to inter-particle interactions, despite not explicitly coupling it with x -direction. Simulations are performed for 20 ns, the first 10 ns data are discarded to allow for a fully developed flow profile, and the next 10 ns data are collected at every 0.2 ps. Ten identical simulations are performed with initial velocities of particles drawn from a Maxwell distribution with different seeds, to get an error estimate on the mean velocity profile. Bins of width $0.1\sigma_{ff}$ are used to compute the density and $0.2\sigma_{ff}$ are used to sample velocity profiles. For reliable statistics, a minimum of 500 fluid particles were simulated in MD system, with box lengths suitably adjusted to account for the correct average density in the channel.

IV. RESULTS

To test the proposed hydrodynamic model, we present here the results for three different types of systems with differing surface–fluid interaction and corrugation. We calculate the density profiles from EQT, which are used in calculating viscous component of the flow. Slip component of the flow is incorporated using Eq. (21). For the low friction system (C–CH₄), fluid inside the slit is in equilibrium with a bath of bulk density (c_b) 2.138 atoms/nm³, whereas moderate friction system (C*–CH₄) is in equilibrium with bulk fluid with density $c_b = 2.936$ atoms/nm³. Finally, the high friction case (Si–CH₄) is at thermodynamic state corresponding to a bulk density $c_b = 2.97$ atoms/nm³. To obtain the values of parameters R_{min} and R_{crit} in Eq. (9), we adopt the linear scaling relations proposed in Ref. 39 as a first approximation. These parameters are then fine tuned to obtain the present results. EQT parameters are reported in Table II. Comparison of the density profiles in Fig. 2 between EQT and MD shows that there is a good quantitative match between the two methods.

Variation of the local average density (\bar{c}) computed from EQT profile using Eq. (13) is also plotted in Fig. 2. We see that the average density is weighted average form of the density, and hence shows less undulations in its profile. There is not much shift in the peak position between the average density and density peaks because of the nature of the chosen weight function, which provides a higher bias for $|z - z'| \rightarrow 0$ as ev-

TABLE II. EQT parameters for computing density profiles.

System	R_{crit} (nm)	R_{min} (nm)	a_0 (kJ/mol)	a_1 (kJ/mol/nm)	a_2 (kJ/mol/nm ²)
C–CH ₄	0.24	0.4125	87.1561	−417.4426	492.9563
C*–CH ₄	0.19	0.4095	99.1396	−475.7608	563.9083
Si–CH ₄	0.19	0.4170	71.4594	−341.7384	401.6761

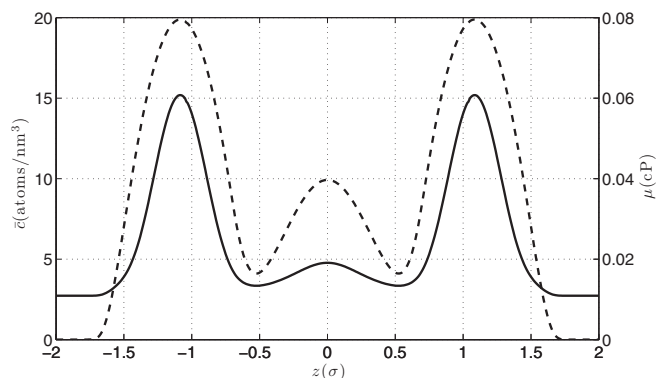


FIG. 3. Average density (dashed line, left-axis) and viscosity (solid line, right-axis) for $4\sigma_{ff}$ wide Si–CH₄ system.

ident from Eq. (13). A representative plot of viscosity profile is presented for Si–CH₄ system in Fig. 3. It should be noted that viscosity in the limit of zero average density ($\bar{c} \rightarrow 0$) is $\mu \rightarrow \mu_0$, which is the dilute gas viscosity.

The autocorrelation integral $\int_0^\infty \langle F(0)F(t) \rangle dt$ is computed from the autocorrelation data $\langle F(0)F(t) \rangle$ obtained from EMD simulation. We assume that the autocorrelation follows exponential relaxation. A two parameter exponential function is fitted to MD autocorrelation data, and further calculations for computing the integral is done on the fitted function. This process is needed for only one slit, since they are independent of slit size, and the results presented in Fig. 4 are for $20\sigma_{ff}$ channel. As evident from the plots, the maximum value of force autocorrelation $\langle F(0)F(0) \rangle$ increases from lowest friction (C–CH₄) case to highest friction case (Si–CH₄), indicating that magnitude of slip velocity should be highest in C–CH₄ system and lowest in Si–CH₄ system, as understood from Eq. (21). The parameters for exponential fit are reported in Table III.

A. Low wall-fluid friction: Methane confined between graphene surfaces

Since the surface energy parameter of graphene is very low ($\epsilon_{ww}/k_B = 28$ K) and it possesses a hexagonal closed packed structure of sp^2 hybridized carbon with bond length of 0.142 nm compared to its diameter of 0.34 nm, its surface landscape is smooth. Therefore, this weakly corrugated surface results in a high degree of specular reflections of fluid particles after interaction with the wall, leading to a very little resistance to the collective motion of fluid under gravity driven flow. This physics is well captured in the results presented in Fig. 5 for various slit sizes, which demonstrate that there is a considerable amount of slip flow, reflected by the plug-like nature of velocity profiles. It can be deduced that

TABLE III. Parameters for exponential fit $\langle F(0)F(t) \rangle \approx A \exp(-Bt)$.

System	A (kJ/mol/nm ²)	B (1/ps)
C–CH ₄	2.256×10^3	15.710
C*–CH ₄	1.186×10^4	12.484
Si–CH ₄	5.722×10^5	16.350

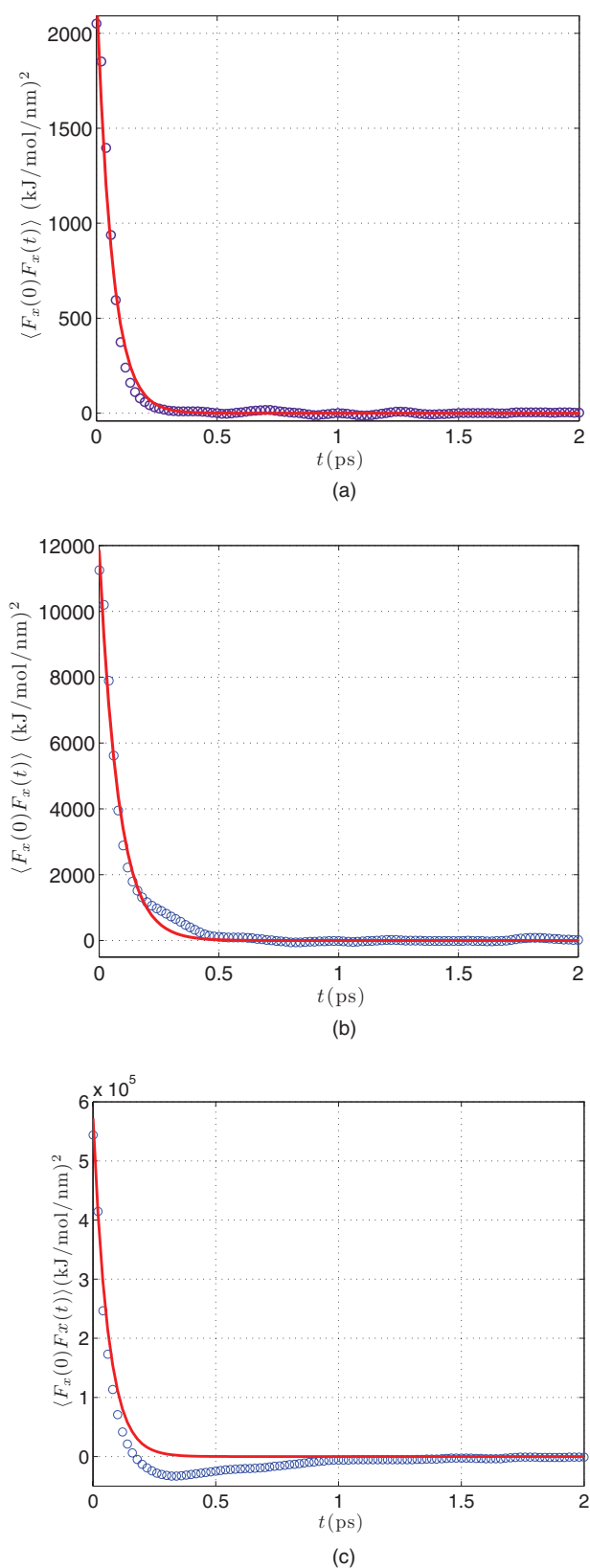


FIG. 4. Surface-fluid total force autocorrelation from MD simulation (circles, blue) and exponential fits (solid line, red) for (a) C-CH₄, (b) C*-CH₄, and (c) Si-CH₄ system.

the viscous effects are not so important in this type of low wall-fluid friction systems. However, the contribution of slip flow decreases with increase in the slit size, where the effect of the wall subsides in the region far away from the interface, and the viscous contribution starts to increase. Slip velocity boundary condition is applied at the first peak of the density profile, which is at a distance of 0.3619 nm from the wall.

B. Moderate wall-fluid friction: Methane confined between modified graphene surfaces

For this system, the LJ potential energy parameter ϵ_{ww} of the wall was set equal to that of the fluid, thereby making the wall-fluid (slip) and fluid-fluid (viscous) effects comparable to each other. The amount of slip observed in response to applied gravity is less than that of graphene-methane system (as applied gravity value for the slip case is about one order of magnitude less than that of the other two cases), but still there is a considerable amount of slip present in the velocity profiles as shown in Fig. 6. This can be explained by increased corrugation of the surface potential, responsible for the degree of slippage. Enhanced value of the wall-fluid interaction energy parameter results in more friction and therefore provides more resistance to the moving fluid, as compared to the low friction case. In this case, a prominent parabolic shaped velocity superimposed on a considerable amount of slip flow for larger slit size is observed (see Fig. 6(a)). We again observe that the effect of slip contribution increases with decreasing slit size, similar to slip case (see Figs. 6(a)–6(d)). This is due to the wall effects becoming dominant in the smaller slit size channels, because the confining surfaces are closer. Again, slip velocity boundary condition is applied at the first peak of the density profile, which is at a distance of 0.3619 nm from the wall.

C. High wall-fluid friction: Methane confined between silicon surfaces

In this case, surface structure (FCC 111, rougher than that of graphene lattice) and wall-fluid interaction energy parameter result in increased corrugation of the potential, which is non-conductive for facilitating slip. A very little amount of slip is observed as shown in Fig. 7. This case is representative of the viscous effects dominating over slip. The velocity profiles show a parabolic type nature in larger size slits as shown in Fig. 7(a), while a non-parabolic velocity profile is clearly evident in Fig. 7(b) for a slit size of $9\sigma_{\text{ff}}$, which shows undulations near the interface. Reducing the slit size further to $4\sigma_{\text{ff}}$, where no bulk type region is observed in the density profile (see Figs. 2(c) and 3), shows significant deviation from parabolic profile as seen from Fig. 7(c) which one would obtain using a constant density and viscosity. Thus, a spatially varying density and viscosity formulation of hydrodynamic problem is important especially in smaller slit sizes. Again, the slip velocity boundary condition is applied at 0.3239 nm, which is the first density peak location. It is observed that the match between continuum and MD results is not so good for $3\sigma_{\text{ff}}$ wide channel. This can be attributed

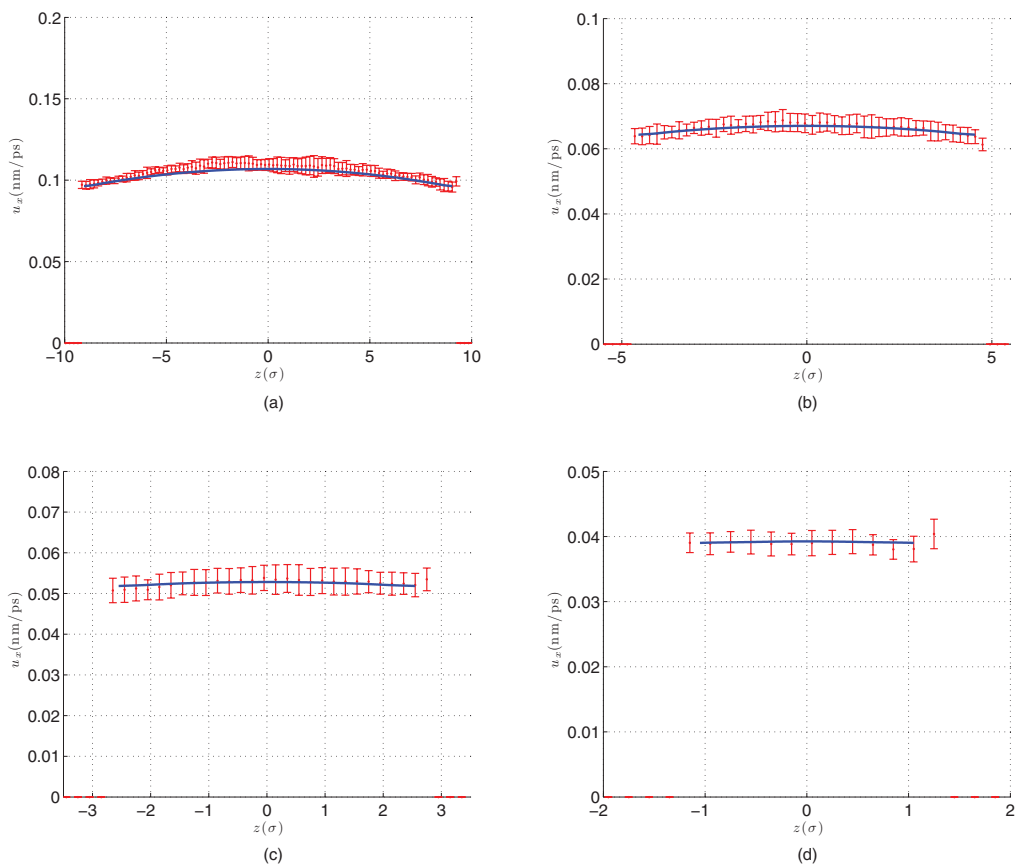


FIG. 5. Velocity profiles for methane confined in graphene slits of size (a) $20\sigma_{FF}$, (b) $11\sigma_{FF}$, (c) $7\sigma_{FF}$, and (d) $4\sigma_{FF}$. Continuum results are in solid line (blue), while MD results are represented by error bars (red).

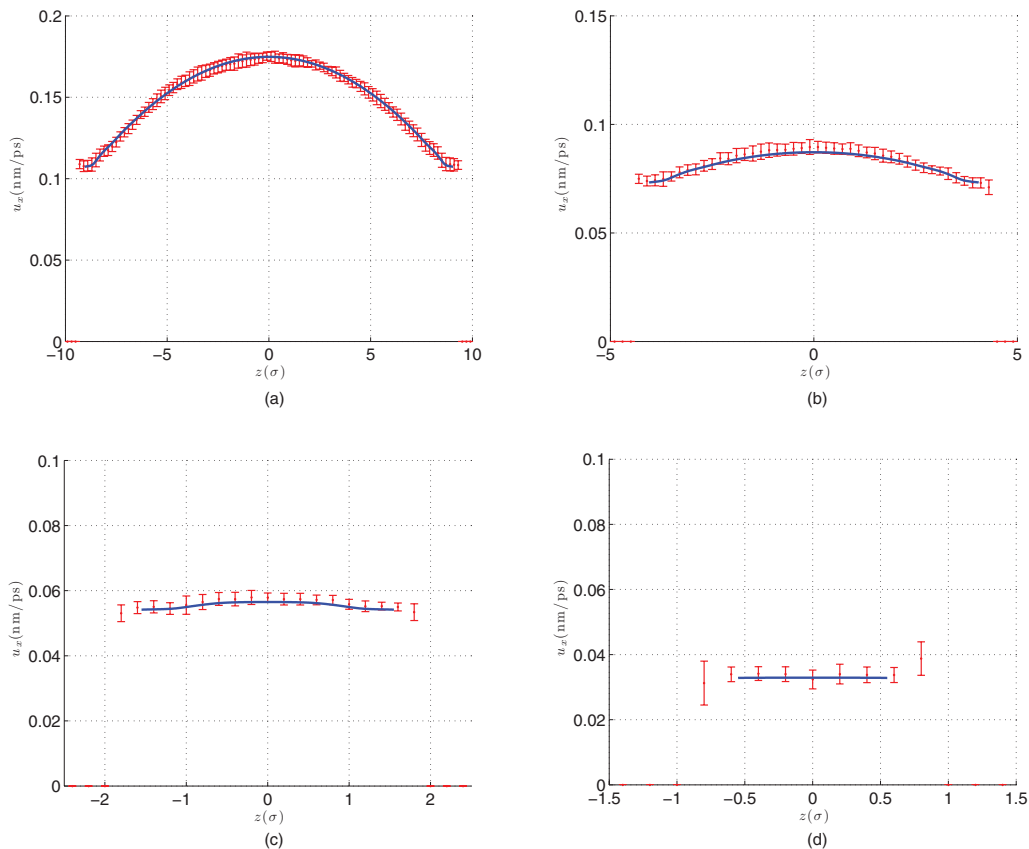


FIG. 6. Velocity profiles for methane confined in modified graphene [C*] slits of size (a) $20\sigma_{FF}$, (b) $10\sigma_{FF}$, (c) $5\sigma_{FF}$, and (d) $3\sigma_{FF}$. Continuum results are in solid line (blue), while MD results are represented by error bars (red).

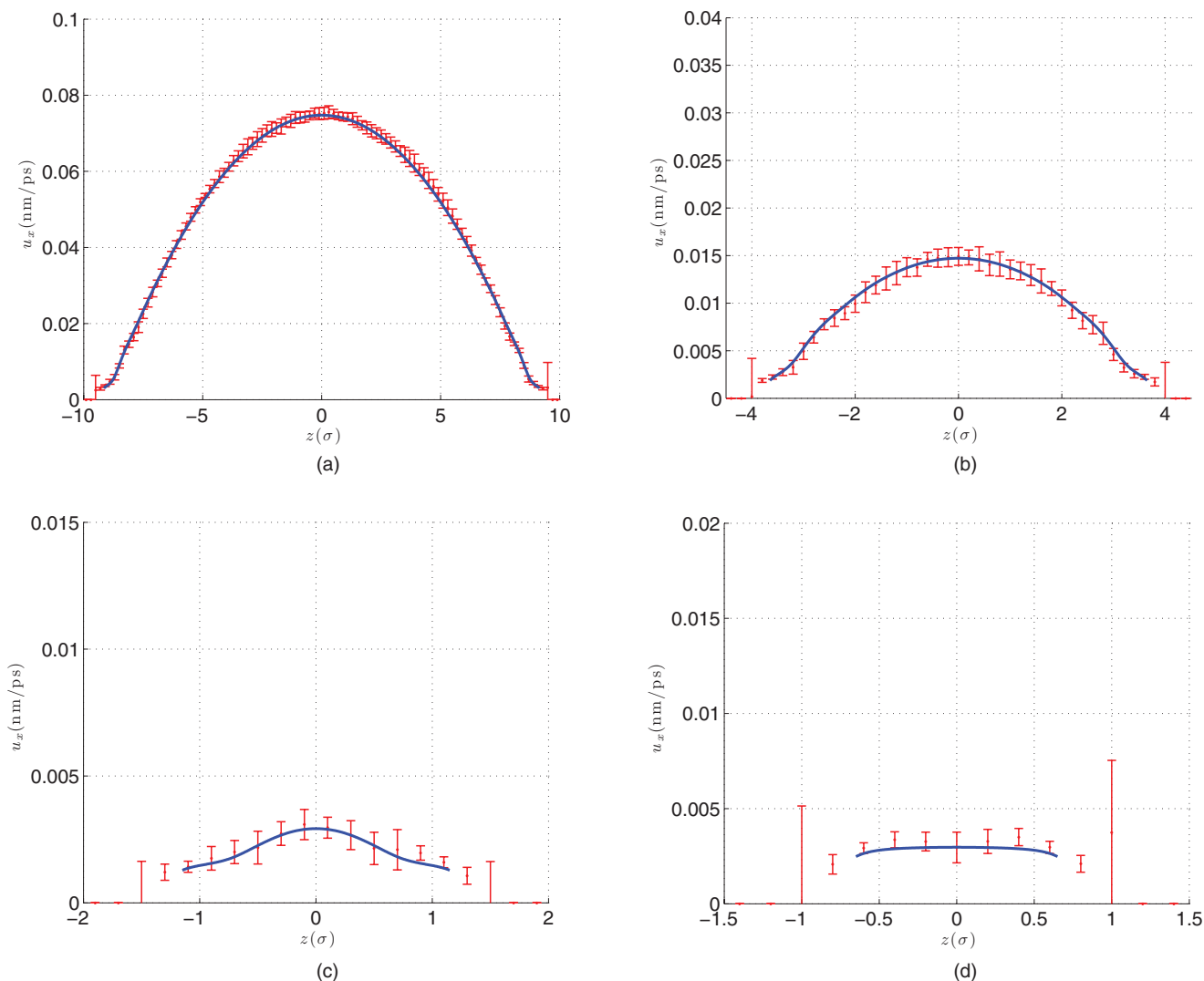


FIG. 7. Velocity profiles for methane confined in silicon slits of size (a) $20\sigma_{ff}$, (b) $9\sigma_{ff}$, (c) $4\sigma_{ff}$, and (d) $3\sigma_{ff}$. Continuum results are in solid line (blue), while MD results are represented by error bars (red).

to the assumption of exponential relaxation for autocorrelation of wall–fluid interaction force (see Fig. 4(c)). A better approximation would capture the backscattering effects in the autocorrelation, thereby reducing the value of the integral and enhanced value of slip, which currently lacks in the present approximation.

D. Mass flow rate

To test the relative contribution of slip and viscous effects in different systems, we calculate the mass flow rate, \dot{m} , as

$$\dot{m} = \int_{-\frac{L}{2} + \delta}^{+\frac{L}{2} - \delta} mc(z)u_x(z)dz. \quad (22)$$

The above equation assumes unit length in y -direction. To compute the slip contribution to the mass flow rate \dot{m}_s , the profile $u_x(z)$ is replaced by a constant value of u_s obtained from Eq. (21). The ratio \dot{m}_s/\dot{m} is calculated for all systems and it is observed from Fig. 8, that the contribution of slip

in mass flow rate is highest in narrower slits. Similar trends are also observed by Bhatia *et al.* in Ref. 64, where the effect of contribution of viscous flow decreases in narrower SWNT (10,10) as compared to larger SWNT (60,60). While viscous effects are important in larger slits and slip starts to become a dominant flow mechanism in narrower slits, the contribution of viscous effects still cannot be neglected since they account for about 30% of flow rate in high friction system at slit size of $4\sigma_{ff}$ (see Fig. 8(b)). A constant density and viscosity based transport model would result in a very different value of mass flow rate, therefore the importance of density and viscosity variations cannot be overlooked in these cases.

V. CONCLUSIONS

In this study, we have developed a quasi-continuum hydrodynamic transport model for gravity driven flow in slit shaped nanopores. We have demonstrated the importance of both viscous and slip components in the velocity profile by considering three different types of systems which elucidate competition between the two phenomenon. Density profiles

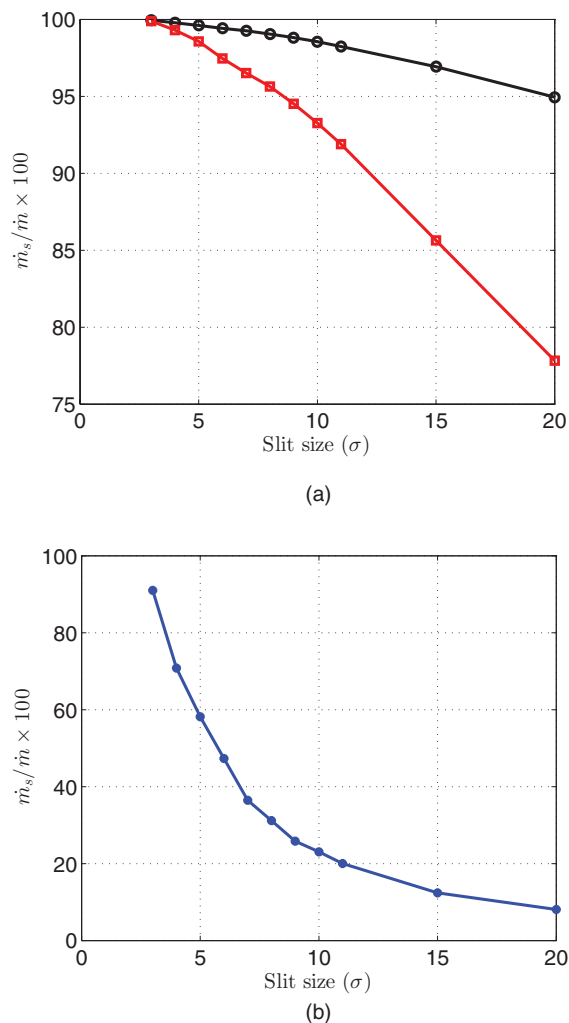


FIG. 8. Percent contribution of slip to mass flow rate (a) C-CH₄ system marked with open circles (black) and C*-CH₄ system with open squares (red) (b) Si-CH₄ system with bold circles. The lines are drawn as a guide to the data points.

are used to calculate space dependent viscosity profile, using LADM method. This variation is necessary to capture the non-parabolic nature of velocity profiles as it would have been for constant density and viscosity case. A general boundary condition which takes into account the total wall-fluid interactions modeled into the static Langevin equation describing center of mass motion of fluid inside the slit is used. It is demonstrated that this boundary condition works for a spectrum of wall-fluid interaction type, and its parameters are constant for fluids confined in slit under same thermodynamic state. Furthermore, it is revealed from the velocity profiles that the slip contribution in mass flow rate increases in all cases when the confining length is decreased, which indicates that wall-fluid effects become more dominant compared to fluid-fluid effects for smaller slit sizes. Overall, this model results in good agreement with the velocity profiles obtained from NEMD simulations, and is valid for reasonable thermodynamic states that are studied in experiments for a variety of wall-surface interactions. Since the present paper deals with low densities, a comprehensive approach would include test-

ing this model for different thermodynamic states to gauge the limits for its applicability.

ACKNOWLEDGMENTS

This work was supported by the NSF (Grant Nos. 0852657 and 0915718). R.B. thanks Sikandar Mashayak and Tarun Sanghi for helpful discussions on EQT. The authors acknowledge the use of the Taub cluster provided by the Computational Science and Engineering Program at the University of Illinois.

- ¹D.-E. Jiang, V. R. Cooper, and S. Dai, *Nano Lett.* **9**, 4019 (2009).
- ²S. Succi, *Phys. Rev. Lett.* **89**, 064502 (2002).
- ³J. D. Figueroa, T. Fout, S. Plasynski, H. McIlvried, and R. D. Srivastava, *Int. J. Greenhouse Gas Control* **2**, 9 (2008).
- ⁴M. A. Shannon, P. W. Bohn, M. Elimelech, J. G. Georgiadis, B. J. Marinas, and A. M. Mayes, *Nature (London)* **452**, 301 (2008).
- ⁵M. E. Suk, A. V. Raghunathan, and N. R. Aluru, *Appl. Phys. Lett.* **92**, 133120 (2008).
- ⁶M. E. Suk and N. R. Aluru, *J. Phys. Chem. Lett.* **1**, 1590 (2010).
- ⁷S. Joseph and N. R. Aluru, *Nano Lett.* **8**, 452 (2008).
- ⁸M. S. P. Sansom and P. C. Biggin, *Nature (London)* **414**, 156 (2001).
- ⁹M. Knudsen, *Ann. Phys.* **333**, 75 (1909).
- ¹⁰M. von Smoluchowski, *Ann. Phys.* **338**, 1559 (1910).
- ¹¹S. K. Bhatia, M. R. Bonilla, and D. Nicholson, *Phys. Chem. Chem. Phys.* **13**, 15350 (2011).
- ¹²I. Bitsanis, J. J. Magda, M. Tirrell, and H. T. Davis, *J. Chem. Phys.* **87**, 1733 (1987).
- ¹³I. Bitsanis, T. K. Vanderlick, M. Tirrell, and H. T. Davis, *J. Chem. Phys.* **89**, 3152 (1988).
- ¹⁴Y. Zhu and S. Granick, *Phys. Rev. Lett.* **88**, 106102 (2002).
- ¹⁵P. A. Thompson and S. M. Troian, *Nature (London)* **389**, 360 (1997).
- ¹⁶X. Yong and L. Zhang, *Microfluid. Nanofluid.* **14**, 299 (2012).
- ¹⁷A. Martini, A. Roxin, R. Q. Snurr, Q. Wang, and S. Lichter, *J. Fluid Mech.* **600**, 257 (2008).
- ¹⁸F.-C. Wang and Y.-P. Zhao, *Soft Matter* **7**, 8628 (2011).
- ¹⁹G. Arya, H.-C. Chang, and E. J. Maginn, *Mol. Simul.* **29**, 697 (2003).
- ²⁰L. Bocquet and J.-L. Barrat, *Soft Matter* **3**, 685 (2007).
- ²¹N. V. Priezjev, *Phys. Rev. E* **75**, 051605 (2007).
- ²²A. Niavarani and N. V. Priezjev, *Phys. Rev. E* **81**, 011606 (2010).
- ²³N. V. Priezjev and S. M. Troian, *J. Fluid Mech.* **554**, 25 (2006).
- ²⁴O. G. Jepps, S. K. Bhatia, and D. J. Searles, *Phys. Rev. Lett.* **91**, 126102 (2003).
- ²⁵O. G. Jepps, S. K. Bhatia, and D. J. Searles, *J. Chem. Phys.* **120**, 5396 (2004).
- ²⁶S. K. Bhatia, O. Jepps, and D. Nicholson, *J. Chem. Phys.* **120**, 4472 (2004).
- ²⁷S. K. Bhatia and D. Nicholson, *J. Chem. Phys.* **127**, 124701 (2007).
- ²⁸Q. Cai, M. J. Biggs, and N. A. Seaton, *Phys. Chem. Chem. Phys.* **10**, 2519 (2008).
- ²⁹G. Arya, H.-C. Chang, and E. J. Maginn, *Phys. Rev. Lett.* **91**, 026102 (2003).
- ³⁰V. P. Sokhan, D. Nicholson, and N. Quirke, *J. Chem. Phys.* **115**, 3878 (2001).
- ³¹V. P. Sokhan, D. Nicholson, and N. Quirke, *J. Chem. Phys.* **117**, 8531 (2002).
- ³²L. Bocquet and J.-L. Barrat, *Phys. Rev. E* **49**, 3079 (1994).
- ³³J.-L. Barrat and L. Bocquet, *Faraday Discuss.* **112**, 119 (1999).
- ³⁴J. Petracic and P. Harrowell, *J. Chem. Phys.* **127**, 174706 (2007).
- ³⁵V. P. Sokhan, D. Nicholson, and N. Quirke, *J. Chem. Phys.* **120**, 3855 (2004).
- ³⁶V. P. Sokhan and N. Quirke, *Mol. Simul.* **30**, 217 (2004).
- ³⁷L. V. Woodcock, *AIChE J.* **52**, 438 (2006).
- ³⁸A. V. Raghunathan, J. H. Park, and N. R. Aluru, *J. Chem. Phys.* **127**, 174701 (2007).
- ³⁹T. Sanghi and N. R. Aluru, *J. Chem. Phys.* **132**, 044703 (2010).
- ⁴⁰T. Sanghi and N. R. Aluru, *J. Chem. Phys.* **136**, 024102 (2012).
- ⁴¹S. Y. Mashayak and N. R. Aluru, *J. Chem. Phys.* **137**, 214707 (2012).
- ⁴²S. Y. Mashayak and N. R. Aluru, *J. Chem. Theory Comput.* **8**, 1828 (2012).
- ⁴³W. A. Steele, *Surf. Sci.* **36**, 317 (1973).
- ⁴⁴H. Hoang and G. Galliero, *J. Chem. Phys.* **136**, 124902 (2012).

- ⁴⁵H. T. Davis, *Statistical Mechanics of Phases, Interfaces and Thin Films* (Wiley, 1996).
- ⁴⁶J. Hansen and I. R. McDonald, *Theory of Simple Liquids* (Elsevier, 2006).
- ⁴⁷T. K. Vanderlick, L. E. Scriven, and H. T. Davis, *J. Chem. Phys.* **90**, 2422 (1989).
- ⁴⁸S. Chapman and T. G. Cowling, *The Mathematical Theory of Non-Uniform Gases; An Account of the Kinetic Theory of Viscosity, Thermal Conduction, and Diffusion in Gases* (Cambridge University Press, 1939).
- ⁴⁹Z. Guo, T. S. Zhao, C. Xu, and Y. Shi, *Int. J. Comput. Fluid Dyn.* **20**, 361 (2006).
- ⁵⁰T. H. Chung, M. Ajlan, L. L. Lee, and K. E. Starling, *Ind. Eng. Chem. Res.* **27**, 671 (1988).
- ⁵¹N. Mehdipour and H. Eslami, *Int. J. Therm. Sci.* **41**, 949 (2002).
- ⁵²G. Ihm, Y. Song, and E. A. Mason, *J. Chem. Phys.* **94**, 3839 (1991).
- ⁵³M. M. Papari, *Chem. Phys.* **288**, 249 (2003).
- ⁵⁴D. G. Friend and J. C. Rainwater, *Chem. Phys. Lett.* **107**, 590 (1984).
- ⁵⁵W. T. Ashurst and W. G. Hoover, *Phys. Rev. A* **11**, 658 (1975).
- ⁵⁶R. Zwanzig, *Nonequilibrium Statistical Mechanics* (Oxford University Press, 2001).
- ⁵⁷R. Kubo, *Rep. Prog. Phys.* **29**, 255 (1966).
- ⁵⁸R. Qiao and N. R. Aluru, *Phys. Rev. Lett.* **92**, 198301 (2004).
- ⁵⁹R. Qiao and N. R. Aluru, *J. Chem. Phys.* **118**, 4692 (2003).
- ⁶⁰I. K. Snook and W. van Megen, *J. Chem. Soc., Faraday Trans. 2* **77**, 181 (1981).
- ⁶¹S. K. Das, M. M. Sharma, and R. S. Schechter, *J. Phys. Chem.* **100**, 7122 (1996).
- ⁶²S. Plimpton, *J. Comput. Phys.* **117**, 1 (1995).
- ⁶³S. Nosé, *J. Chem. Phys.* **81**, 511 (1984).
- ⁶⁴S. K. Bhatia, H. Chen, and D. S. Sholl, *Mol. Simul.* **31**, 643 (2005).